

Supplementary Information

Colloidal particle deposition on microchannel walls, for attractive and repulsive surface potentials

T. Porto Santos^{*,a,b,‡}, R. Lopes Cunha^a, P. Tabeling^b, and C.M. Cejas^{*,b,‡}

^a Department of Food Engineering, Faculty of Food Engineering, University of Campinas, Rua Monteiro Lobato, 80-CEP 13083-862 Campinas, Brazil

^b Microfluidics, MEMS, Nanostructures Laboratory, CNRS Chimie Biologie Innovation (CBI) UMR 8231, Institut Pierre Gilles de Gennes (IPGG), ESPCI Paris, PSL Research University
6 rue Jean Calvin 75005, Paris, France

[‡] Authors contributed equally to this work

* Corresponding authors: tatiana.porto90@gmail.com, cesare.cejas@gmail.com

A Particle ζ potential measurements using ZetaSizer

The ζ potentials of all colloidal particles used in the experiments (PS-plain, PS-fluo, and PS-amine) are measured using a ZetaSizer Nano Series (Malvern Instruments, UK). Beforehand, the colloidal particles are sonicated (Branson 2800) and diluted in deionized water (1:10000), followed by their insertion inside a zeta cell (DTS1070). The measurements are performed in triplicate. We determine the ζ_p for PS-fluo, PS-plain, and PS-amine particles as a function of C_{salt} . The results are presented in the Fig. 1.

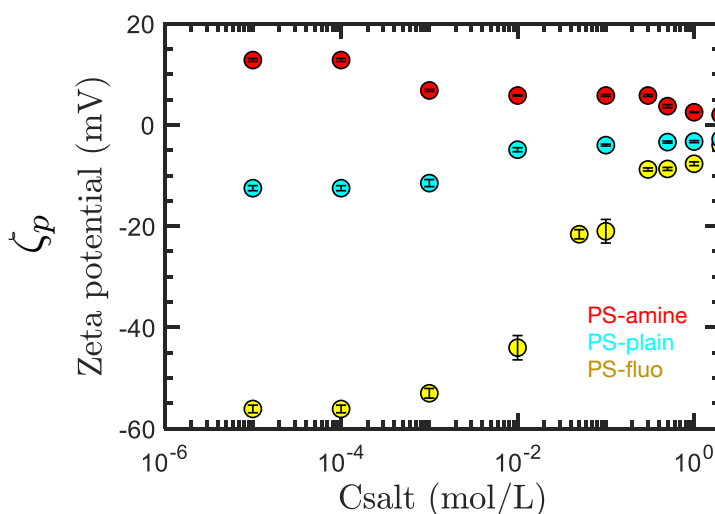


Figure 1: Plot of ζ_p for PS-fluo (●), PS-plain (●), and PS-amine (●) as function of C_{salt} obtained using the Zetasizer.

All three curves exhibit a sigmoidal pattern where there is minimal change at low salt concentrations, followed by a transition, then a constant value at high salt concentrations.

PS-amine exhibits a slightly positive charge due to the amine molecules grafted onto the surface. Thus, ζ_p has a smaller value at high ionic strengths and increases positively at lower ionic strengths.

Both PS-plain and PS-fluo exhibit negative surface charges and thus ζ_p has a lower value (in terms of mag-

nitude) almost close to zero at high ionic strengths while ζ_p becomes increasingly negative at lower ionic strengths. PS-fluo has a higher surface charge density due to the carboxylate anions. This explains why the ζ_p for PS-fluo is more negative than that of PS-plain, which is not specifically functionalized.

From our experimental measurements, we find that the ζ_p value decreases slowly at low salt concentrations. In some cases, such as PS-plain, the ζ_p value does not vary significantly within two orders of magnitude of low salt concentration.

B Information on numerical simulations

As mentioned in the main manuscript, we perform simulations by expressing the advection-diffusion equation in terms of Langevin equations [1, 2, 3, 4] of the form:

$$\dot{\mathbf{r}}_i(t) = \frac{\mathbf{D}_i \mathbf{F}_i}{kT} + \nabla \cdot \mathbf{D}_i + \mathbf{U}(\dot{\mathbf{r}}_i) + \Delta(t) \quad (1)$$

where $\dot{\mathbf{r}}_i$ is the vector position of the i th particle with respect to time, \mathbf{D}_i is the anisotropic diffusion, \mathbf{F}_i is the total force acting on the particle, k is the Boltzmann constant, T is temperature, \mathbf{U} is the contribution of the flow to the particle speed, and $\Delta(t)$ takes into account the random Brownian displacement, equivalent to $\sqrt{2D\tau}$. In non-complex geometries, such as a straight rectangular channel, these quantities are documented in literature. The time derivatives are replaced by a first order discretization. Ideally, τ (simulation time step) should be as small as possible. However, taking an even smaller value of τ greatly increases computing times. In practice, the values we take for τ range between $0.5 \cdot 10^{-6}$ s and $1.5 \cdot 10^{-5}$ s, which are well below the characteristic times of the problem. We verify that the results are insensitive to the particular value of τ taken within this range.

The Lagrangian approach also makes it easier to compute the Langevin equation, i.e. determining particle trajectory by writing that particle speed is equal to the force applied on it times its mobility [5, 6]. Thus, by applying these general equations to the particular geometry we consider, i.e. long shallow channels with rectangular cross-sections, where geometry is invariant in the y direction, we obtain the following:

$$\dot{x}(t) = \gamma(z)U(z) + \beta_x(z)\delta(t) \quad (2)$$

$$\dot{z}(t) = \beta_z(z)\delta(t) + \frac{d\beta_z}{dz}D + \beta_z \frac{D}{kT} (F_{vdWz} + F_{elz}) \quad (3)$$

where $\dot{x}(t)$ and $\dot{z}(t)$ are vector positions of the particle with respect to time respectively in the x (along the length of the channel) and z (along the height of the channel) directions. The \dot{x} component of the particles, moving along the channel length, have a unidirectional flow speed, scaled by γ . The trajectory along x has a correction factor, β_x , expressing confinement of the particle diffusion coefficient [6]. The \dot{z} component of the particles expresses the trajectory along z dimension with a diffusion component, whose correction factor, β_z , changes with particle distance with respect to the wall.

The expressions for $\dot{y}(t)$ and β_y convey similar forms [6, 7] respectively to that of $\dot{z}(t)$ and β_z but is ultimately negligible since we only consider the trajectories of the particles along x (length) and z (height), i.e. we analyze the deposition on the channel ceiling and floor, at $z \pm \frac{h}{2}$, and neglect the particles on the sidewalls.

In the following subsections, we provide a description of each of the terms in Eq.2 and Eq.3.

B.1 Calculation of γ

The parameter γ introduces the ratio between average flow speed and the particle speed near the wall when $z \approx r$ [7, 8, 9]:

$$\gamma(\eta) = \frac{U_p(z)}{U_r} \quad (4)$$

where where $U_p(z)$ is the average flow speed of the Poiseuille profile, $U_r = \frac{6Qr}{wh^2} \left(1 - \frac{r}{h}\right)$ is the flow speed at $z \approx r$, where r is particle radius. The parameter $\gamma(\eta)$ has the following expression as function of η , where $\eta = \frac{z-r}{r}$. For $\eta > 1$,

$$\gamma(\eta) = 1 - \frac{5}{16\eta^3} \quad (5)$$

for $10^{-4} < \eta < 1$,

$$\gamma(\eta) = \frac{1}{\eta + 1} \exp(0.68902 + \log(\eta) + 0.072332 \log^2(\eta) + 0.0037644 \log^3(\eta)) \quad (6)$$

for $\eta < 10^{-4}$,

$$\gamma(\eta) = \frac{0.7431}{0.6376 - 0.2 \log(\eta)} \quad (7)$$

We introduce the coordinate:

$$\bar{\eta} = \int_0^\eta \eta \gamma(\eta) d\eta \quad (8)$$

In the case where van der Waals interactions dominate, for example, where $z - r$ (and thus η) is relatively small, this solution is not convenient to use, instead opting for an approximate solution by treating $\gamma(\eta)$ as a constant, $\gamma(\eta) \sim \gamma^*$. With this approximation, we obtain:

$$\bar{\eta} \approx \frac{\gamma^*}{2} \eta^2 \quad (9)$$

Comparison between the approximate (Eq.8) and the exact solutions (Eq.9), same as in Ref. [7], show that by treating, for example, $\gamma^* = 0.7$, the approximate solution is barely indistinguishable from the exact one within a given range of η between 10^{-3} and 1 (Fig.2). In physical terms, this corresponds to 2.5nm and $2.5\mu\text{m}$. Simulations show that below 2.5nm, all of the particles immediately adsorb to the wall, and consequently, the error made on the speed of deposition does not impact significantly the final position of the particle, nor the time it takes for getting adsorbed to the wall.

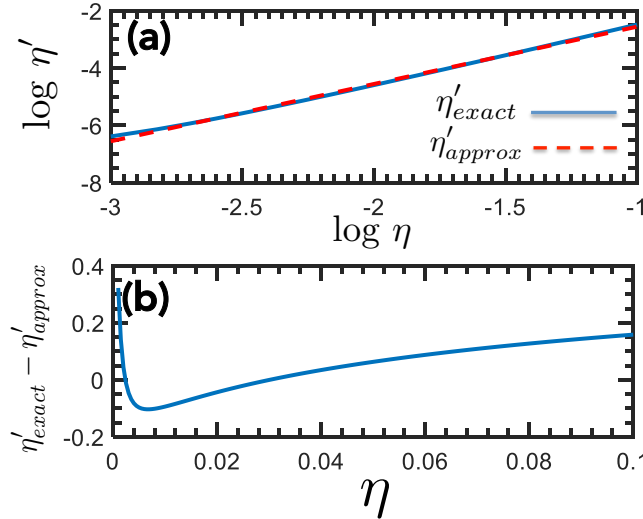


Figure 2: (a) Comparison, on a log log plot, between the approximate expression $\bar{\eta} = \frac{\gamma^*}{2} \eta^2$ with $\gamma^* = 0.7$ and the exact solution $\bar{\eta} = \int_0^\eta \eta \gamma(\eta) d\eta$. (b) Plot of the difference $\int_0^\eta \eta \gamma(\eta) d\eta - \frac{\gamma^*}{2} \eta^2$ as a function of η .

B.2 β_x and β_z

The parameters $\beta_x(z)$ and $\beta_z(z)$ are dimensionless functions expressing the dependence of the longitudinal and transverse particle diffusion coefficients with z , the initial position of the particle with respect to the wall. From literature, the expressions for β_x and β_z are as follows [6, 3, 8, 9]:

$$\beta_x = 1 - \frac{9}{16z} + \frac{1}{8z^3} - \frac{45}{256z^4} - \frac{1}{16z^5} \quad (10)$$

$$\beta_z = \frac{6z^2 - 10z + 4}{6z^2 - 3z - 1} \quad (11)$$

B.3 $\delta(t)$

As the particles move in the direction of the channel length, x , $\delta(t)$ is a zero mean step random function with amplitude $\sqrt{2D\tau}$, where τ is the discrete incremental step used to calculate the trajectories. The parameter $\delta(t)$ is an analogue to $\Delta(t)$ in Eq.1. This parameter is in fact well-established [10] to take the Brownian movement into account. This makes the equation stochastic and as a result very difficult to solve, except in the case where this term can be neglected.

B.4 Contribution of other forces

The bulk diffusion coefficient of the particles is represented by the Stokes-Einstein coefficient, D , while F is the force acting on the particle, comprising of two components: van der Waals, F_{vdWz} , and electrostatic forces, F_{elz} . Both forces act on the z direction, perpendicular to the wall.

$$F_{vdWz} = -\frac{Ar}{6(z-r)^2} \text{ and } F_{elz} = \frac{\chi}{\lambda_D} \exp\left(-\frac{z-r}{\lambda_D}\right) \quad (12)$$

The Hamaker constant, A , defines the strength of the surface interactions and can be affected by significant surface roughness [11]. We only consider Hamaker constant values where $A > 0$. The parameter χ is a dimensionless function showing the product of the ζ potential values:

$$\chi = 4\pi\epsilon\epsilon_0\zeta_w\zeta_p r \quad (13)$$

in which ϵ , ϵ_0 are respectively the relative dielectric constant of the fluid transporting the particles and the permittivity of free space, ζ_w and ζ_p are respectively the zeta potentials of the channel wall and the particle, and r is particle radius. Here, we consider both conditions where $\chi > 0$ (repulsive charges or similar ζ signs) and $\chi < 0$ (attractive charges or opposite ζ signs).

The parameter λ_D is the Debye length, (also expressed as κ^{-1}), which for a monovalent salt follows [12]:

$$\lambda_D = \kappa^{-1} = \sqrt{\frac{\epsilon\epsilon_0 kT}{2(N_{Av})e^2 I}} \quad (14)$$

where N_{Av} is Avogadro's number, e is the elementary charge, and I is the ionic strength (mol/m^3) equivalent to salt concentration in molarity, C_{salt} .

B.5 Contribution of surface roughness

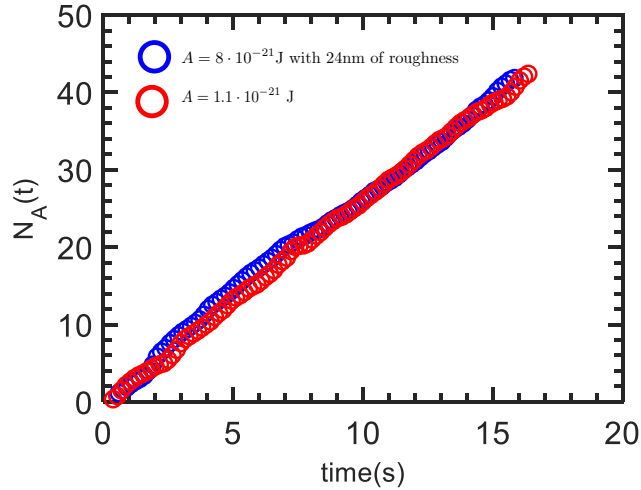


Figure 3: (a) Numerical simulation results of $N_A(t)$ for $A = 1.1 \cdot 10^{-21}$ J, which provides the same result as $A = 8.0 \cdot 10^{-21}$ J with $R_q = 24\text{nm}$.

Surface roughness, R_q , affects surface interactions. Notably, it has been shown [13, 11] that Hamaker constants can vary with a certain degree of surface roughness but are often complex to analytically describe. Hence, surface roughness is usually characterized using AFM. In the theoretical analysis in the main manuscript, we did not introduce any surface roughness effect. This could have been done by modifying extensively the expression of the van der Waals forces but owing to simplicity, we did not do it. In the numerical simulations, however, the roughness effect can be gauged by incorporating it into the particle-surface distance, z , thereby resulting to a total effective particle-surface distance of $z + R_q$.

Take for example PDMS and unfunctionalized particles (PS-plain), in which both are considered smooth or with negligible roughness, the Hamaker constant for this interaction was determined to be $A = 8.0 \cdot 10^{-21}$ J [7, 5,

14]. If we keep PDMS as the surface and change the particles from PS-plain to PS-fluo, we know that the Hamaker constant for this interaction was experimentally measured to be $A = 1.1 \cdot 10^{-21}$ J. Using this A value agrees well with simulations. Moreover, in the simulation for this case, R_q was set to 0 since we presume that any obtained A value from the experiments already takes into account the effect of any roughness.

Furthermore, in Fig. 3, we find that the simulation results for $A = 1.1 \cdot 10^{-21}$ J (red circles) is also equivalent to the results of $A = 8.0 \cdot 10^{-21}$ J but with an additional 24 nm surface roughness (blue circles). In this regard, this suggests that the functionalization of PS-fluo adds a roughness value that changes the Hamaker constant from $A = 8.0 \cdot 10^{-21}$ J to an effective value of $A = 1.1 \cdot 10^{-21}$ J.

B.6 Glossary of parameters and constants used in the theory and simulation section

Table 1: Nomenclature

Symbol	Definition
h	channel height
w	channel width
L	channel length
C	particle concentration in the advection-diffusion equation
U_p	average velocity based on Poiseuille profile
U_r	flow velocity at distance $z \approx r$
\dot{x}	vector position in the x direction
\dot{z}	vector position in the z direction
γ	ratio between U_p/U_r
β_x	dimensionless function expressing dependence of longitudinal particle diffusion coefficient w.r.t wall
β_z	dimensionless function expressing dependence of transverse particle diffusion coefficient w.r.t wall
$\delta(t)$	zero mean step random function with amplitude, $\sqrt{2D\tau}$
τ	incremental time step
D	Stokes-Einstein diffusion coefficient of particle
A	Hamaker constant
r	particle radius
k	Boltzmann constant
T	temperature
χ	dimensionless function showing product strength of ζ_w and ζ_p
ζ_w	zeta potential of the microfluidic channel surface walls
ζ_p	zeta potential of the colloidal particle surface
ϵ	dielectric constant of the fluid
ϵ_0	permittivity of free space
λ_D	Debye length
N_{Avo}	Avogadro's number
e	elementary charge
C_{salt}	salt concentration in molar units
I	ionic strength in mol/m ³ units
F_{vdWz}	van der Waals forces which act on the z direction perpendicular to wall
F_{elz}	electrostatic forces which act on the z direction perpendicular to wall
S	collection factor
z_0	position of the particle w.r.t wall following its exit trajectory
η	dimensionless altitude, $\eta = \frac{(z-r)}{\lambda_D}$, but in definition of $\gamma(\eta)$, η is also dimensionless altitude $\eta = \frac{(z-r)}{r}$
t	time
P	dimensionless parameter showing strength of van der Waals forces w.r.t Debye forces
σ_L	dimensionless parameter equivalent to $\sigma_L = \frac{D\chi L}{\gamma_0 U_r \lambda_D r k T}$
ξ_L	effective Peclet number
Q	flow rate (velocity \times cross section)
φ	experimental particle concentration
v_p	spherical volume of the particle
$N_A(t)$	number of adsorbed particles as a function of time
S_{vdw}	theoretical expression of S when van der Waals forces dominate (at high ionic strengths)

C Numerical simulations of ζ_w and ζ_p for repulsive charges

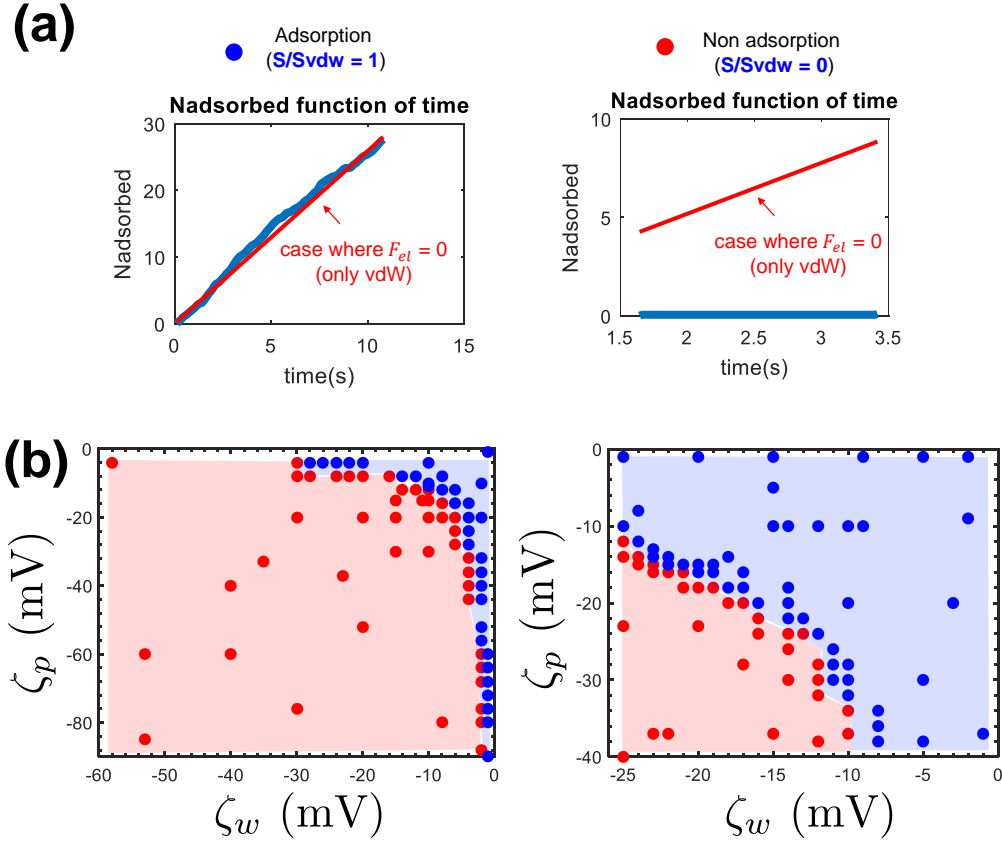


Figure 4: **(a)** Simulation results based on Langevin equations with adhesion and electrostatic forces. In the case of repulsive charges, results are binary, i.e. deposition/adsorption (●) or no deposition/adsorption (●). When $S/S_{vdw} = 1$, the simulation results agree with the theoretical expression, which has been calculated at conditions of high ionic strengths where van der Waals forces control deposition and electrostatic contributions are inexistent. When $S/S_{vdw} = 0$, the simulation results do not agree with the theoretical expression, mainly because simulation results show that particles are repelled from the surface. This happens at lower salt concentrations. **(b)** Some examples of different combinations of ζ_p and ζ_w for a certain salt concentration. **(b, left)** 0.01 M NaCl and **(b, right)** 0.1M NaCl. Blue and red regions represent deposition and no deposition, respectively.

We perform numerical simulations based on Langevin equations and generate a phase diagram of ζ_p and ζ_w combinations. In this case, for repulsive charges, both ζ_w and ζ_p have the same sign. The sign is negative (-) for both to mirror that of the typical surface charge under aqueous conditions.

As described, we perform numerical simulations of particle deposition on the microchannel surface taking into account contributions of the different forces such as adhesion (vdW) and electrostatic (Debye). Generally, at a given C_{salt} , there is a certain ζ_p and ζ_w . However, depending on the type of particle or channel wall surface, we can also have various combinations of both ζ potentials. In these simulations results shown in Fig. 4, we demonstrate different combinations of ζ_p and ζ_w , where results seem to be binary, i.e. deposition/adsorption (●) or no deposition/non-adsorption (●). This binary result also explains why S/S_{vdw} is either 0 or 1. When $\frac{S}{S_{vdw}} = 1$, this means that the S value obtained from simulations is equivalent to the theoretical expression, S_{vdw} , represented by the solid red line in Fig. 4(a, left). This is the theoretical prediction at high salt concentration, typically at concentrations ≥ 0.1 M NaCl, where deposition is controlled by van der Waals-adhesion forces and electrostatic forces, $F_{el} \approx 0$.

When $\frac{S}{S_{vdw}} = 0$, this means that the S value from simulations is zero as in Fig.4(a, right), i.e. particles are repelled from the surface and thus there is no deposition.

For reference, S is from Eq.16 and S_{vdw} is from Eq.13 in the main manuscript.

Results in Fig. 4(b) show that for a wide range of values, the deposition result does not change significantly, i.e. the particles are either attracted (●) to or repelled (●) from the surface. In this example, both ζ_w and ζ_p possess the same sign (repulsive charges).

Two examples are given in the figure: 0.01M NaCl in Fig. 4(b, left) and 0.1M NaCl in Fig. 4(b, right). In both cases, any combination of ζ_p and ζ_w that falls within the red zone means that both surface charges repel each other. Hence, the particle does not deposit onto the surface. For example, at 0.1M NaCl, a $\zeta_w = -15\text{mV}$ and $\zeta_p = -30\text{mV}$ combination would yield no deposition. However, a combination $\zeta_w = -20\text{mV}$ and $\zeta_p = -5\text{mV}$ will result to deposition.

We have also evaluated literature data (e.g. in Ref. [15, 16]) on ζ_p and ζ_w combinations and the results indeed fall within the shaded region.

D Numerical simulations of ζ_w and ζ_p for attractive charges

We perform additional numerical simulations based on Langevin equations (see Theory and Simulations section in main manuscript; see also Ref. [7, 5, 14]) and generate diagrams of ζ_p , ζ_w , and S/S_{vdw} combinations. In this case, for attractive charges, both ζ_w and ζ_p have the opposite sign.

As described in the main manuscript, we perform numerical simulations of particle deposition on the microchannel surface taking into account contributions of the different forces such as adhesion (vdW) and electrostatic (Debye). At a given C_{salt} , we have already experimentally determined ζ_p from ZetaSizer measurements (see SI-A).

Knowing the value of ζ_p and keeping it constant, we vary ζ_w over a wide range (from -100 mV to +100 mV). We further extend the analyses by performing more simulations at two additional (hypothetical) ζ_p values. Similarly, we keep these hypothetical ζ_p values constant while also varying ζ_w over an identical range (-100mV to +100mV). Results are shown in Fig. 5 (PS-fluo and APTES-treated PDMS) and Fig. 6 (PS-amine and plasma-treated PDMS).

The results in Fig. 5 show simulations for PS-fluo (-) on APTES-treated walls (+), taking into account $A = 1 \cdot 10^{-21}$ J, as determined experimentally.

Results in Fig. 5 reveal a sigmoidal pattern, where at (-) values of ζ_w , $S/S_{vdw} = 0$. This is expected since the particle, PS-fluo, has a negative charge. Thus, two negative surface charges result to repulsion. There is a transition value at low ζ_w values, followed by a plateau. Simulations show that for wide range of (+) ζ_w values spanning approximately two orders of magnitude, from $\sim +1$ mV to +100mV, the value of S/S_{vdw} does not significantly change. For example, at 0.01M NaCl (Fig.5(c)) and $\zeta_p = -44$ mV (red circle), a ζ_w value of either $\zeta_w = +18$ mV or $\zeta_w = +100$ mV, yields approximately the same value for $S/S_{vdw} \approx 1.5$.

In the case of attractive charges, $S/S_{vdw} \approx 1$ only at higher salt concentrations, 0.1M NaCl (Fig. 5(d)) and 1M NaCl (Fig. 5(e)). For lower ionic strengths, $S/S_{vdw} \gg 1$, as also predicted by our experiments. The qualitative trend of increasing deposition at low ionic strengths agrees with experiments, although there is disparity between the actual quantitative values at low salt concentrations (see Experiments: attractive charges section in main manuscript). Our experiments generally predict a smaller S/S_{vdw} value, probably due to the fact that the simulation does not take into account interparticle interactions once the experiment saturates (too many particles that result to aggregation)

The results in Fig. 6 show simulations for PS-amine (+) on hydrophilic plasma-treated walls (-), taking into account $A = 0.4 \cdot 10^{-21}$ J, as determined experimentally.

Results in Fig. 6 also reveal a sigmoidal pattern but in reverse, where at (+) values of ζ_w , $S/S_{vdw} = 0$. This is expected since the particle, PS-amine, has a positive charge. Thus, two positive surface charges also result to repulsion. There is a transition value at low negative ζ_w values, followed by a plateau at increasingly negative ζ_w values.

Simulations show that for wide range of (-) ζ_w values spanning approximately from ~ -1 mV to -100 mV, the value of S/S_{vdw} does not significantly change. For example, at 0.001M NaCl (Fig.6(b)) and $\zeta_p = +6.8$ mV (red circle), a ζ_w value of either $\zeta_w = -25$ mV or $\zeta_w = -100$ mV, yields approximately the same value for $S/S_{vdw} \approx 5$.

Similar to the previous case for attractive charges, $S/S_{vdw} \approx 1$ only at higher salt concentrations, 0.1M NaCl (Fig. 6(d)) and 1M NaCl (Fig. 6(e)). For lower ionic strengths, $S/S_{vdw} \gg 1$, as also predicted by our experiments. Similarly, the qualitative trend of increasing deposition at low ionic strengths agrees with experiments, although there is still disparity between the actual quantitative values at low salt concentrations.

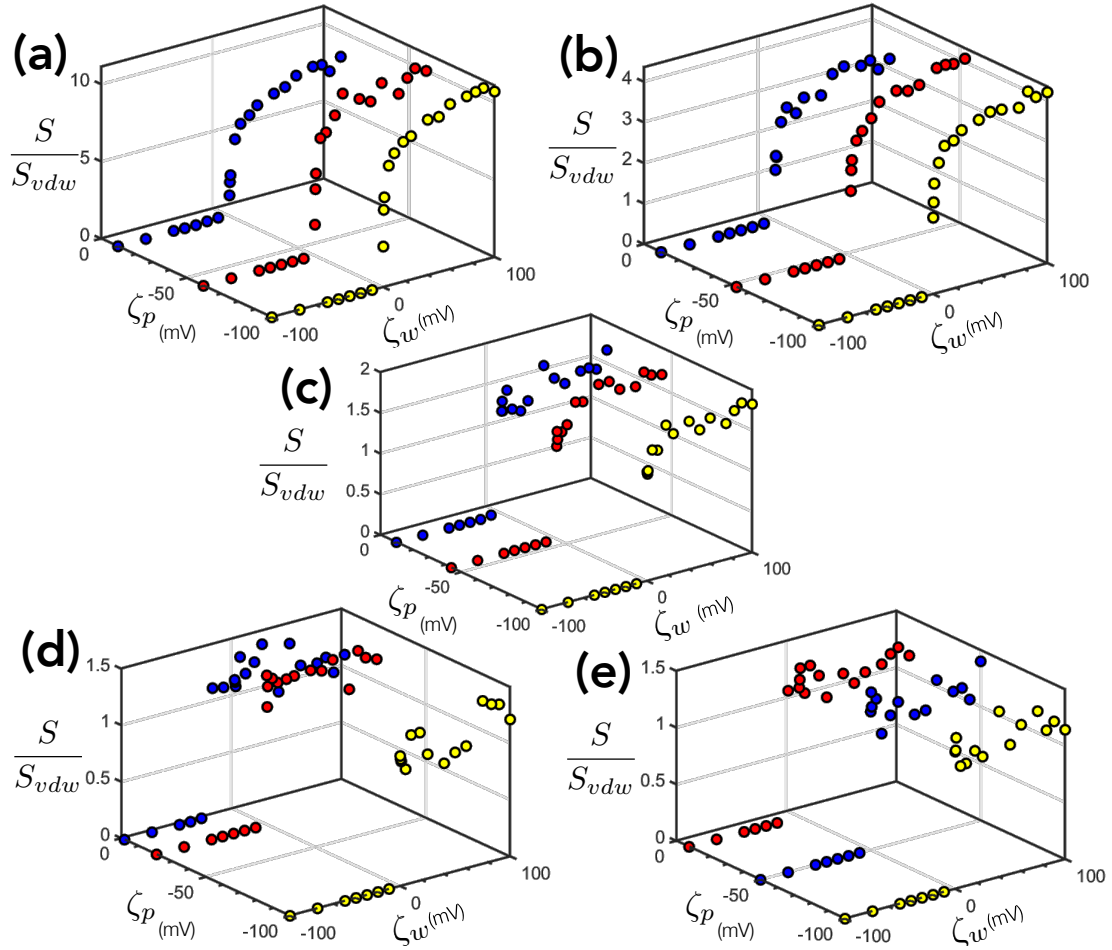


Figure 5: Simulation results based on Langevin equations with adhesion and electrostatic forces for PS-fluo and APTES-treated wall, where surface charges have opposite signs. (a) Results at 0.0001M NaCl. (b) Results at 0.001M NaCl. (c) Results at 0.01M NaCl. (d) Results at 0.1M NaCl. (e) Results at 1M NaCl. In (a-e) (●) are the experimental ζ_p values obtained from the ZetaSizer, while (●) and (●) are two hypothetical ζ_p values at $\zeta_p = -10$ mV and $\zeta_p = -100$ mV respectively. However, in (e) (●) and (●) are two hypothetical ζ_p values at $\zeta_p = -50$ mV instead and $\zeta_p = -100$ mV respectively.

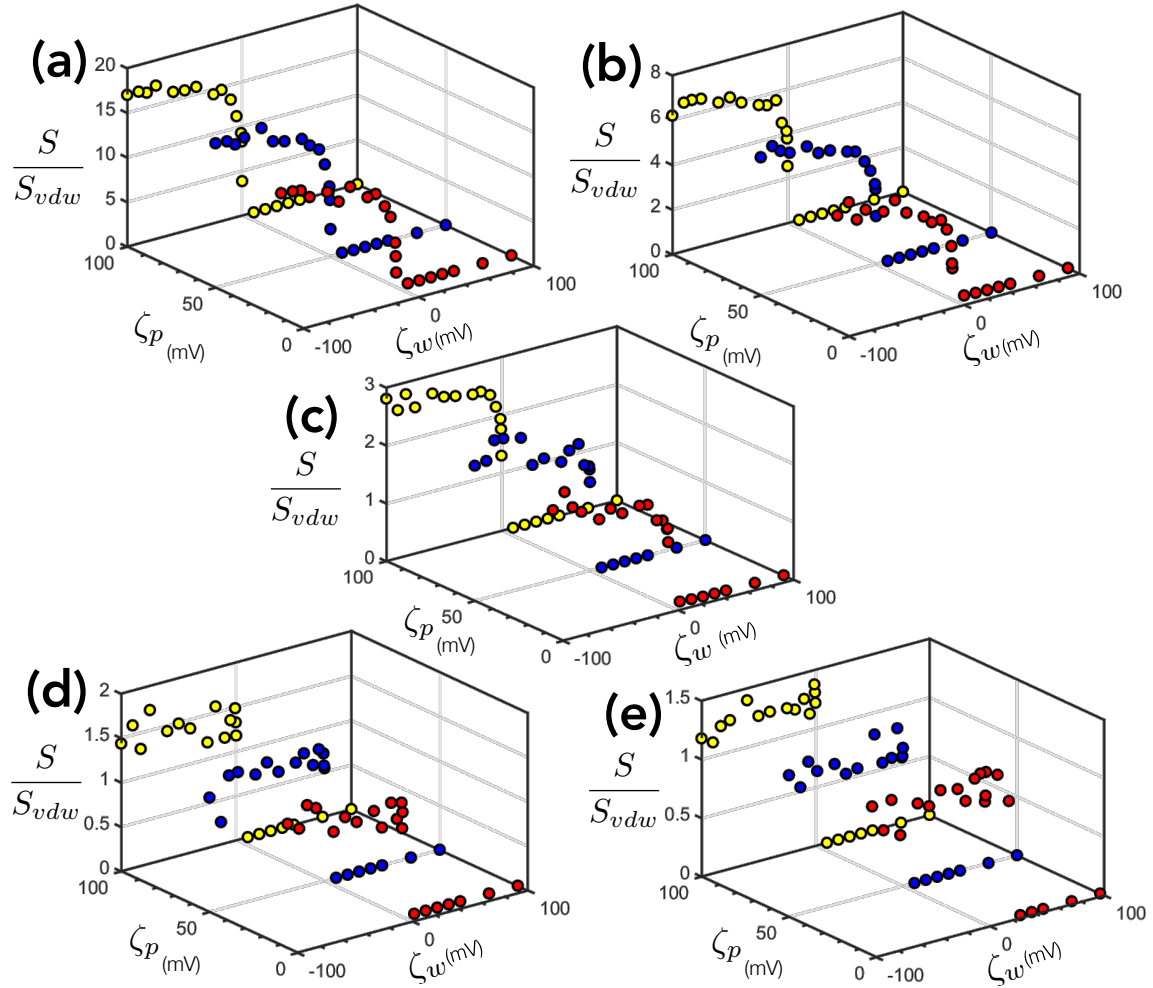


Figure 6: Simulation results based on Langevin equations with adhesion and electrostatic forces for PS-amine and plasma-treated wall, where surface charges have opposite signs. (a) Results at 0.0001M NaCl. (b) Results at 0.001M NaCl. (c) Results at 0.01M NaCl. (d) Results at 0.1M NaCl. (e) Results at 1M NaCl. In (a-e) (●) are the experimental ζ_p values obtained from the ZetaSizer, while (●) and (●) are two hypothetical ζ_p values at $\zeta_p = +50\text{mV}$ and $\zeta_p = +100\text{mV}$ respectively.

E Experimental and numerical results for $N_A(t)$ at different ionic strengths for attractive charges

We perform numerous comparisons of experimental and numerical results, in which some examples are shown in Fig. 7 for the number of particles adsorbed as a function of time, $N_A(t)$ at different salt concentrations.

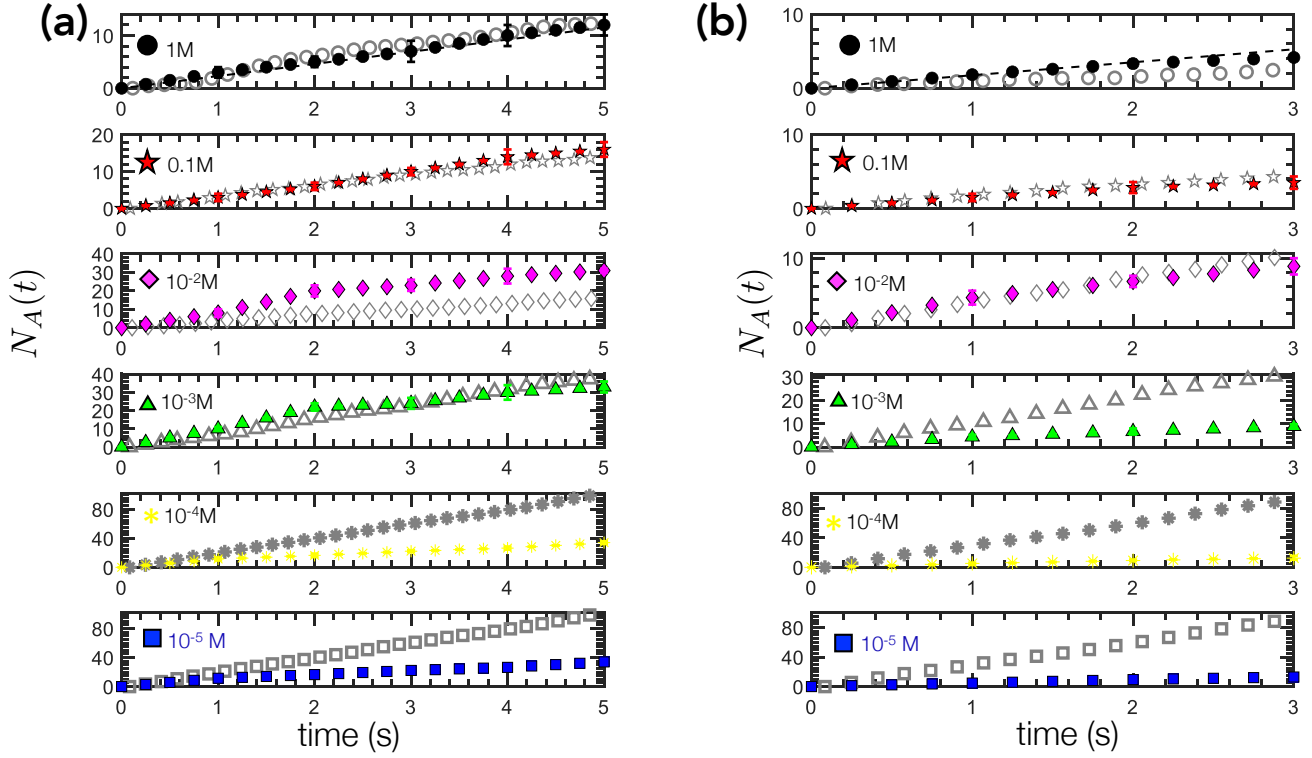


Figure 7: Simulation and experimental results of $N_A(t)$ at different salt concentrations during initial seconds of deposition. (a) Results for PS-fluo on APTES-treated wall, where $A = 1.1 \cdot 10^{-21}$ J, $r = 2.4 \mu\text{m}$, $U = 8 \text{mm/s}$, ζ_p varies accordingly to the graph in Fig.1 (SI-A), and $\zeta_w = +1 \text{mV}$ for 10^{-2} M to 1M NaCl, $\zeta_w = +25 \text{mV}$ for 10^{-3} M to 10^{-5} M NaCl. (b) Results for PS-amine on plasma-treated wall, where $A = 0.4 \cdot 10^{-21}$ J, $r = 2.4 \mu\text{m}$, $U = 8 \text{mm/s}$, ζ_p varies accordingly to the graph in Fig.1 (SI-A), and $\zeta_w = -1 \text{mV}$ for 10^{-2} M to 1 M NaCl, $\zeta_w = -10 \text{mV}$ for 10^{-3} M to 10^{-5} M NaCl.

At high salt concentrations, surface charges are screened so their magnitudes are typically smaller while at lower salt concentrations, the magnitude of the charges are larger. From simulations concerning different ζ_w values (SI-C and SI-D) for these two different surface treatments, it appears that from a certain value, any further increase in the magnitude of the ζ_w no longer has a significant effect on the number of adsorbed particles since the curve of S/S_{vdw} begins to plateau.

References

- [1] C. Henry, P. Minier, and G. Lefevre, “Towards a description of particulate fouling: from single particle deposition to clogging,” *Adv. Colloids Inter. Sci.*, vol. 185–186, pp. 34–76, 2012.
- [2] H. Unni and C. Yang, “Kinetics of colloidal particle deposition to a solid surface from pressure driven microchannel flows,” *Can. J. Chem. Engr.*, vol. 85, pp. 609–616, 2007.
- [3] —, “Colloidal particle deposition from electrokinetic flow in microfluidic channel,” *Electrophoresis*, vol. 30, pp. 732–741, 2009.
- [4] Z. Adamczyk, T. Dabros, J. Czarnecki, and T. V. de Ven, “Particle transfer to solid surfaces,” *Adv. Colloids Inter. Sci.*, vol. 19, pp. 183–252, 1983.
- [5] C. M. Cejas, F. Monti, M. Truchet, J. Burnouf, and P. Tabeling, “Universal diagram for the kinetics of particle deposition in microchannels,” *Physical Review E*, vol. 98, p. 062606, 2018.
- [6] P. Tabeling, *Introduction to Microfluidics*. Oxford, UK: Oxford University Press, 2005.
- [7] C. M. Cejas, F. Monti, M. Truchet, J. Burnouf, and P. Tabeling, “Particle deposition kinetics of colloidal particles in microchannels at high ionic strength,” *Langmuir*, vol. 33, no. 26, pp. 6471–6480, 2017.
- [8] H. Brenner, “The slow motion of a sphere through a viscous fluid towards the plane,” *Chem. Eng. Sci.*, vol. 16, pp. 242–251, 1961.
- [9] M. Bevan and D. Prieve, “Hindered diffusion of colloidal particles very near to the wall: revisited,” *J. Chem. Phys.*, vol. 113, pp. 1228–1236, 2000.
- [10] P. Huang and K. Breuer, “Direct measurement of anisotropic near-wall hindered diffusion using total internal reflection velocimetry,” *Phys. Rev. E*, vol. 76, no. 046307, 2007.
- [11] M. C. Stevenson, S. P. Beaudoin, and D. S. Corti, “Toward an improved method for determining the hamaker constant of solid materials using atomic force microscopy. i. quasi-static analysis for arbitrary surface roughness,” *J. Phys. Chem. C*, vol. 124, pp. 3014–3027, 2020.
- [12] A. Khair and T. M. Squires, “The influence of hydrodynamic slip on the electrophoretic mobility of a spherical colloidal particle,” *Physics of Fluids*, vol. 21, p. 042001, 2009.
- [13] V. Valmacco, M. Elzvbieciak-Wodka, C. Besnard, P. Maroni, G. Trefalt, and M. Borkovec, “Dispersion forces acting between silica particles across water: influence of nanoscale roughness,” *Nanoscale Horiz.*, vol. 1, p. 325, 2016.
- [14] C. M. Cejas, L. Maini, F. Monti, and P. Tabeling, “Deposition kinetics of bi- and tridisperse colloidal suspensions in microchannels under the van der waals regime,” *Soft Matter*, vol. 15, p. 7438, 2019.
- [15] A. Garg, C. Cartier, K. Bishop, and D. Velegol, “Particle zeta potentials remain finite in saturated solutions,” *Langmuir*, vol. 32, pp. 11 837–11 844, 2016.
- [16] B. Mustin and B. Stoeber, “Single layer deposition of polystyrene particles onto planar polydimethyl siloxane substrates,” *Langmuir*, vol. 32, pp. 88–101, 2016.